Influence of core property on multi-electron process in slow collisions of isocharged sequence ions with neon*

Lu Rong-Chun(卢荣春)[a)b)], Yu De-Yang(于得洋)[a)†], Shao Cao-Jie(邵曹杰)[a)], Ruan Fang-Fang(阮芳芳)[a)], and Cai Xiao-Hong(蔡晓红)[a)]

[a)] *Institute of Modern Physics, Chinese Academy of Sciences, Lanzhou* 730000, *China*
[b)] *Graduate School of the Chinese Academy of Sciences, Beijing* 100049, *China*

(Received 18 November 2009; revised manuscript received 9 April 2010)

Influence of core property on multi-electron process in the collisions of $q = 6$–9 and 11 isocharged sequence ions with Ne is investigated in the keV/u region. The cross-section ratios of double-, triple-, quadruple- and total multi-electron processes to the single electron capture process as well as the partial ratios of different reaction channels to the relevant multi-electron process are measured by using position-sensitive and time-of-flight techniques. The experimental data are compared with the theoretical predictions including the extended classical over-barrier model, the molecular Columbic barrier model and the semi-empirical scaling law. Results show a core effect on multi-electron process of isocharge ions colliding with Neon, which is consistent with the results of Helium we obtained previously.

Keywords: isocharged sequence ions, multi-electron process, classical over-barrier model
PACC: 5220H, 3450H, 3470

1. Introduction

Multi-electron charge transfer is the main process in the collision of slow highly-charged ions (HCIs) with neutral atoms. It is a many-body collision model with multiple open reaction channels in the quantum mechanical approach. Owing to the advent of electron cyclotron resonance ion source (ECRIS) and the electron beam ion source (EBIS) in the past few decades, many efforts have been made to understand its complex dynamics. It is also of fundamental interest for fusion research and astrophysics.[1−9] An early review article introduced the basic concepts and investigations of multiply charged ions with neutral atoms.[10] The knowledge on the mechanisms of multiple captures by HCIs colliding with an atom was extensively described and the multi-electron charge transfer has been focused on since then.[11]

The efforts to perform the experimental research on multi-electron process in the collision of HCIs with neutral atoms were further made with the development of new experimental techniques,[11−13] such as event coincidence and energy–gain spectroscopy. Absolute cross sections for multi-electron processes in low energy (1.8q keV) Ar^{q+} (q = 4–8)-Ar collisions were measured and compared with the extended classical barrier model (ECBM) by Bárány *et al.*[14] The multi-electron capture ($\Delta q = 2 - 6$) emission cross sections of Kr^{18+}–Kr, Ar collisions at 360-keV energy were measured by Martin *et al.*[15] The observation of the branching ratios of the multiply-excited product ions suggested that more electrons could be emitted by spontaneous ionisation from the product ions with the occupied high n levels. It was consistent with theoretical investigations by Vaeck and Hansen[16] and van der Hart and Hansen.[17] Multi-electron transfer probabilities in 90-keV Ne^{9+}–Ne collisions were obtained with respect to the projectile scattering angle in a range of 12–75 mrad by Herrmann *et al.*[4] The absolute cross sections for i-electron capture (to projectile) and j-electron removal (from target), total electron capture, j-electron removal, i-electron capture in 1.5q keV I^{q+} ($q = 10, 15$)–Ne, Ar, Kr and Xe collisions were reported in Ref. [18]. The absolute multi-electron transfer cross sections and branching ratios of product ions in 1.5q keV I^{q+} ($10 \leq q \leq 20$)–Ar, Xe collisions were experimentally determined by Sakaue *et al.*[19] Their result showed multi-electron emission was dominant after three- and four-electron transfers and more electrons could be emitted through multiple spontaneous ionisation from the product ions when higher Rydberg states were occupied and the projectile ion charge was large. Knoop *et al.*[20] investigated double-electron processes. They observed the

*Project supported by the National Natural Science Foundation of China (Grant Nos. 10874188 and 10775160).
†Corresponding author. E-mail: d.yu@impcas.ac.cn
© 2010 Chinese Physical Society and IOP Publishing Ltd

unexpected creation of Na^{3+} ions and explained them into two-electron capture accompanied by ionisation. Multi-electron transfer processes in low energy collisions of bare Kr, Ar and Ne ions with neutral gas target were believed to play a significant role in shaping the K-shell x-ray spectrum.[21] The measurements of charge-state correlations of scattered ions and recoil ions in close collisions of slow Ne^{q+} (q = 1–9) ions with Ar atoms were carried out by Hoshino *et al.*[22] It was found that the mean charge of the ion pairs and the number of captured electrons increased almost linearly with the incident charge q, while the number of ejected electrons from the collision system was independent of q at both 5 and 14 keV.

In the meantime, a few theoretical models were proposed and compared with the experimental results.[3,5,10,11,23–30] Multi-electron transition processes including electron capture, ionisation and Auger were discussed by Janev and Presnyakov.[10] A well-known classical over-barrier model was proposed by Bohr and Lindhard,[31] and then developed for the calculation of absolute cross sections for multi-electron process in slow collisions of HCIs with atoms by Bárány *et al.*[14] and by Niehaus.[3] A theory based on the quantal two-channel molecular orbital close-coupling expansion method well described the measured differential double charge transfer cross sections in the collision of C^{4+} with He.[23] Kimura *et al.*[25] then investigated the partial and total multi-electron capture cross sections in slow collisions of HCIs with atoms within the scaling law based on the extended classical over-barrier model (ECBM). The experimental cross sections were reproduced satisfactorily. Selberg *et al.*[27] presented the semi-empirical scaling laws (SSLs) and compared this expression favourably with the experimental results for slow Xe^{q+} ($15 \leq q \leq 43$) ions colliding with He, Ar and Xe. Additionally, the cross sections of two-electron transitions in slow ion–atom collisions[32] were estimated by a method based on the shake-off mechanism.

The further investigations on the charge transfer of more than two electrons were limited both in the experimental and theoretical approaches despite the previous successes stated above, which is mainly due to the difficulties in the quantum mechanical treatment of many-body scattering with multiple reaction channels.[6,7,11,18,19,22,33] The measurements of the cross section ratios of double-, triple-, quadruple- and the total multi-electron processes to the single electron capture process in $^{13}C^{6+}$–Ne and Ar collisions in the energy range of 4.15–11.08 keV were reported.[6,7] On the other hand, the classical over-barrier models cannot distinguish different ions in an isocharge sequence since the core properties of projectile are neglected. Therefore, the projectile core dependence of multi-electron process in slow collisions of HCIs with atoms is far from being understood. The studies on the contributions of multi-electron processes to inner-shell charge transfer and vacancy production in collisions of bare nuclei with argon were conducted by Becker *et al.*[34] They found that the dependence of the charge transfer cross section on the projectile charge Z_p was weaker than Z_p^5 in the Oppenheimer–Brinkman–Kramers (OBK) approximation. The investigations of absolute (n, l) subshell-selective electron capture and emission cross sections in slow collisions of C^{6+}, O^{6+} with He were carried out by Beijers *et al.*[35] They found the influence of the projectile core on the capture process. de Nijs *et al.*[36] observed a charge-state distribution difference between light ions C^{6+}, N^{6+}, Ne^{6+}, and heavy ions Ar^{6+}, Kr^{6+} in keV-energy collisions of isocharge sequence of ions A^{6+} with Ar, which was caused by the interaction between capture electrons and projectile inner-shell electrons. Fléchard *et al.*[37] found that the symmetric $4l$ and $4l'$ configurations took place principally in two steps by independent-electron (IE) interactions through the $n = 4$ single capture channel by means of the combined experimental/theoretical study of the collisions of Ne^{10+} with He in the $50 \leq q \leq 150$ keV impact energy range. Bernard *et al.*[38] made an isocharge study of multi-electronic capture and stabilization in slow collisions of Ar^{16+}, Xe^{16+}, Kr^{16+} with C^{60} and found that the projectile core effect could increase collision processes with active electron number increasing.

In this work we report on the experiment studies of the same-velocity isocharge ions A^{q+} (q = 6–9 and 11) colliding with He, Ne and Ar and the measurements of the cross-section ratios of double-, triple-, quadruple- and total multi-electron processes to the single electron capture process as well as the partial ratios among different reaction channels, by using position sensitive and time-of-flight techniques. This experiment can conduce to the understanding of the influence of projectile core properties on the multi-electron charge transfer processes in greater details.[1,39,40] The experimental results are compared with those obtained from the classical over-the-barrier models (the molecular Columbic barrier model (MCBM) and ECBM) and the semi-empirical

scaling law (SSL). These models have been described in detail in Ref. [3], so we will not mention them here anymore.

2. Experiment

The experiment was carried out on the 14.5 GHz ECRIS described in Ref. [1]. HCI beam was extracted from the ion source. Their energy and charge state were selected by a dipole magnet and a 64° coaxial electrostatic selector. The ion beam was collimated to a size of about 0.3 mm×0.3 mm by two groups of two-dimensional (2D) collimators, and then transmitted through the target chamber. A high-purity (99.999%) neon gas jet was introduced through a needle at a right angle to the beam direction and interacted with the projectiles in the centre of the target chamber. The target gas flow was controlled by a system of an INFICON VDE016 valve, a TPR265 barometer, and a VCC500 controller. The flowrate was controlled under 3×10^5 Pa·L/s. The vacuum pressure in the collision region was better than 10^{-3} Pa and those in the other regions were higher than 10^{-5} Pa in order to satisfy the single-collision condition for electron transfer, which was described in detail in Ref. [1]. The recoil ions extracted and accelerated by a time-of-flight (TOF) spectrometer, were detected by a microchannel plate detector. The charge states of the scatter ions were analysed by a parallel-plate electrostatic field and then determined by a position-sensitive channel plate detector. The reaction events were discriminated by coincidence, and the TOF spectra of the scattered and recoil ions were measured by an MPA-3 multi-parameter acquisition system.

The charge state q of isocharged sequence ions were 6 (C^{6+}, N^{6+}, O^{6+}, F^{6+}, Ne^{6+}, Ar^{6+}, and Ca^{6+}), 7 (O^{7+}, F^{7+}, Ne^{7+}, S^{7+}, and Ar^{7+}), 8 (F^{8+}, Ne^{8+}, Ar^{8+}, and Ca^{8+}), 9 (F^{9+}, Ne^{9+}, Si^{9+}, S^{9+}, Ar^{9+}, and Ca^{9+}) and 11 (Si^{11+}, Ar^{11+}, and Ca^{11+}). Their velocities are to be the same for each ion sequence in order to show the core effect. However, ECRIS voltage which can vary from 10 kV to 25 kV, limits the velocity selection of isocharge sequence ion. In order to test the effect of velocity, we have measured the TOF spectra of $q = 6$ sequence of ions (C^{6+}, N^{6+}, and O^{6+} at $0.49v_0$ and F^{6+}, Ne^{6+} at $0.35v_0$ and at both velocities) and $q = 7$ sequence of ions (F^{7+}, Ne^{7+}, and S^{7+} at $0.43v_0$ and Ar^{7+}, Ca^{7+} at $0.42v_0$ and $0.40v_0$).

The experimental uncertainties mainly come from the statistical error of the multi-electron process, the efficiency difference of the PSMCP detector, and the uncertainty of the counting region in the 2D spectrum. The statistical error is less than ±10%, and the difference detection efficiency is within ±10%, and the counting uncertainty is less than ±10%.

3. Results and discussion

The multi-electron process of isocharge ion sequence A^{q+}–Ne can be described as

$$A^{q+} + Ne \rightarrow A^{(q-i)+} + Ne^{j+} + (j-i)e + h\nu, \quad (1)$$

where A^{q+} ion first obtains j electrons from Ne atom, then i electrons are stabilised on the projectile and $(j-i)$ electrons are ionised into the continuum. Here, some terminologies such as the number of electrons captured by projectile and the number of electrons ionised into the continuum have been used. When $(j-i) = 0$, reaction (1) is the pure electron-capture process, i.e., single-electron capture (SC), double-electron capture (DC), triple-electron capture (TC), quadruple-electron capture (QC) etc. When $(j-i) > 0$, reaction (1) describes the transfer ionisation where both capture and ionisation coexist. For example, $Ci\mathrm{I}(j-i)$ means that i electrons of Ne are captured by the projectile and $(j-i)$ electrons from the target are ejected into the continuum. The multi-electron process is defined by the number of active electrons j, such as double-electron (2E) process, triple-electron (3E) process, and quadruple-electron (4E) process and quintuple-electron (5E) process. Total multi-electron (ME) process is defined as being all process except SC. More than 5 electron process, i.e., 5E process, will not be discussed here due to the lack of experimental data.

The cross-section ratios $\sigma^{k\mathrm{E}}/\sigma^{\mathrm{SC}}$ (k = 2–4) for q = 6–9 and 11 isocharge sequence ions colliding with Ne, are calculated by using MCBM, ECBM and SSL models, and the results may be found in Table 1. Since these models cannot predict the transfer ionisation process, the relative partial cross sections of 2E, 3E and 4E processes cannot be calculated using the theoretical models. And the experimental data in this work are shown in Tables 2–6. ME process and the partial reaction channels of different ME process will be discussed in Subsections 3.1 and 3.2 respectively. It should be noted that all three prediction values listed in sequence are corresponding to the three models, i.e., MCBM, ECBM and SSL respectively.

Table 1. Cross-section ratios $\sigma^{k\mathrm{E}}/\sigma^{\mathrm{SC}}$ (k = 2–4) for q = 6–9 and 11 isocharge sequence ions colliding with Ne, calculated by using MCBM, ECBM and SSL models.

q	model	$\sigma^{2\mathrm{E}}/\sigma^{\mathrm{SC}}/(\%)$	$\sigma^{3\mathrm{E}}/\sigma^{\mathrm{SC}}/(\%)$	$\sigma^{4\mathrm{E}}/\sigma^{\mathrm{SC}}/(\%)$	$\sigma^{5\mathrm{E}}/\sigma^{\mathrm{SC}}/(\%)$
6	MCBM	54.5	33.0	13.6	15.8
	ECBM	50.2	35.2	13.8	9.8
	SSL	55.4	34.7	19.7	14.6
7	MCBM	55.0	32.3	18.6	7.0
	ECBM	50.0	35.7	13.5	9.3
	SSL	55.4	34.7	19.7	14.6
8	MCBM	55.3	31.8	18.6	11.8
	ECBM	50.0	36.0	13.3	9.1
	SSL	55.4	34.7	19.7	14.6
9	MCBM	55.5	32.4	18.5	13.7
	ECBM	49.9	36.2	13.2	9.0
	SSL	55.4	34.7	19.7	14.6
11	MCBM	55.3	33.4	17.3	14.8
	ECBM	49.8	36.5	13.1	8.9
	SSL	55.4	34.7	19.7	14.6

Table 2. Experimental cross-section ratios of $\sigma^{k\mathrm{E}}/\sigma^{\mathrm{SC}}$ ($k = 2$–4) for $q = 6$ isocharged sequence ions colliding with neon.

projectile	C^{6+}	N^{6+}	O^{6+}	F^{6+}	F^{6+}	Ne^{6+}	Ne^{6+}	Ar^{6+}	Ca^{6+}
configuration	bare	$1s^1$	$1s^2$	$1s^22s^1$	$1s^22s^1$	$1s^22s^2$	$1s^22s^2$	$[Ne]3s^2$	$[Ne]3s^23p^2$
energy/(keV/u)	6	6	6	6	3	6	3	3	3
velocity v_0	0.49	0.49	0.49	0.49	0.35	0.49	0.35	0.35	0.35
$\sigma^{\mathrm{DC}}/\sigma^{\mathrm{SC}}$	0.027±0.01	0.012±0.005	0.053±0.02	0.039±0.02	0.033±0.02	0.028±0.01	0.03±0.01	0.49±0.05	0.18±0.02
$\sigma^{\mathrm{C1I1}}/\sigma^{\mathrm{SC}}$	0.14±0.02	0.22±0.03	0.17±0.02	0.33±0.03	0.36±0.04	0.46±0.05	0.52±0.05	0.083±0.01	0.057±0.01
$\sigma^{2\mathrm{E}}/\sigma^{\mathrm{SC}}$	0.17±0.02	0.23±0.03	0.22±0.03	0.37±0.04	0.39±0.04	0.49±0.05	0.55±0.05	0.57±0.05	0.24±0.02
$\sigma^{\mathrm{TC}}/\sigma^{\mathrm{SC}}$	0.002±0.001	0.002±0.001	0.039±0.01	0.027±0.01	0.01±0.005	0.008±0.005	0.005±0.003	0.034±0.01	0.047±0.01
$\sigma^{\mathrm{C2I1}}/\sigma^{\mathrm{SC}}$	0.096±0.02	0.074±0.01	0.097±0.02	0.066±0.02	0.065±0.02	0.046±0.02	0.051±0.02	0.023±0.01	0.024±0.01
$\sigma^{\mathrm{C1I2}}/\sigma^{\mathrm{SC}}$	0.041±0.01	0.062±0.01	0.008±0.005	0.007±0.004	0.009±0.005	0.009±0.005	0.009±0.005	0.002±0.001	0.001±0.001
$\sigma^{3\mathrm{E}}/\sigma^{\mathrm{SC}}$	0.14±0.02	0.14±0.01	0.14±0.02	0.10±0.02	0.084±0.02	0.063±0.02	0.065±0.02	0.059±0.02	0.072±0.02
$\sigma^{\mathrm{QC}}/\sigma^{\mathrm{SC}}$	–	–	–	–	–	–	–	–	–
$\sigma^{\mathrm{C3I1}}/\sigma^{\mathrm{SC}}$	0.004±0.002	0.013±0.005	0.049±0.01	0.048±0.01	0.022±0.01	0.014±0.005	0.012±0.005		
$\sigma^{\mathrm{C2I2}}/\sigma^{\mathrm{SC}}$	0.039±0.01	0.04±0.01	0.007±0.004	–	–	–	–	–	–
$\sigma^{\mathrm{C1I3}}/\sigma^{\mathrm{SC}}$	–	–	–	–	–	–	–	–	–
$\sigma^{4\mathrm{E}}/\sigma^{\mathrm{SC}}$	0.043±0.01	0.053±0.01	0.056±0.01	0.048±0.01	0.022±0.01	0.014±0.005	0.012±0.005	–	–

Table 3. Experimental cross-section ratios of $\sigma^{k\mathrm{E}}/\sigma^{\mathrm{SC}}$ ($k = 2$–4) for $q = 7$ isocharged sequence ions colliding with neon.

projectile	O^{7+}	F^{7+}	Ne^{7+}	S^{7+}	Ar^{7+}	Ca^{7+}
configuration	$1s^1$	$1s^2$	$1s^22s^1$	$1s^22s^22p^5$	$[Ne]3s^1$	$[Ne]3s^2p^1$
energy/(keV/u)	4.67	4.67	4.67	4.67	4.38	3.99
velocity v_0	0.43	0.43	0.43	0.43	0.42	0.40
$\sigma^{\mathrm{DC}}/\sigma^{\mathrm{SC}}$	–	0.016±0.01	0.035±0.02	0.096±0.05	0.35±0.05	0.17±0.02
$\sigma^{\mathrm{C1I1}}/\sigma^{\mathrm{SC}}$	0.50±0.08	0.43±0.08	0.49±0.08	0.28±0.05	0.095±0.02	0.046±0.01
$\sigma^{2\mathrm{E}}/\sigma^{\mathrm{SC}}$	0.50±0.08	0.45±0.08	0.53±0.08	0.38±0.07	0.45±0.05	0.22±0.02
$\sigma^{\mathrm{TC}}/\sigma^{\mathrm{SC}}$	0.004±0.003	0.005±0.003	0.003±0.002	0.01±0.005	0.007±0.005	0.005±0.003
$\sigma^{\mathrm{C2I1}}/\sigma^{\mathrm{SC}}$	0.01±0.005	0.027±0.02	0.053±0.02	0.21±0.02	0.029±0.01	0.053±0.01
$\sigma^{\mathrm{C1I2}}/\sigma^{\mathrm{SC}}$	–	–	0.015±0.005	0.033±0.01	0.002±0.002	–
$\sigma^{3\mathrm{E}}/\sigma^{\mathrm{SC}}$	0.01±0.005	0.032±0.02	0.071±0.02	0.25±0.03	0.038±0.01	0.058±0.01
$\sigma^{\mathrm{QC}}/\sigma^{\mathrm{SC}}$	–	–	–	–	–	–
$\sigma^{\mathrm{C3I1}}/\sigma^{\mathrm{SC}}$	–	0.026±2	–	–	0.002±0.002	0.082±0.02
$\sigma^{\mathrm{C2I2}}/\sigma^{\mathrm{SC}}$	0.016±0.005	–	0.003±0.002	–	–	–
$\sigma^{\mathrm{C1I3}}/\sigma^{\mathrm{SC}}$	–	–	–	–	–	–
$\sigma^{4\mathrm{E}}/\sigma^{\mathrm{SC}}$	0.016±0.005	0.026±0.02	0.003±0.002	–	0.002±0.002	0.082±0.02

Table 4. Experimental cross-sections ratios of $\sigma^{k\mathrm{E}}/\sigma^{\mathrm{SC}}$ ($k = 2$–4) for $q = 8$ isocharged sequence ions colliding with neon.

projectile	F^{8+}	Ne^{8+}	Ar^{8+}	Ca^{8+}
configuration	$1s^1$	$1s^2$	[Ne]	$[Ne]3s^2$
energy/keV	4	4	4	4
velocity v_0	0.4	0.4	0.4	0.4
$\sigma^{\mathrm{DC}}/\sigma^{\mathrm{SC}}$	0.027±0.02	0.021±1	0.061±0.02	0.075±0.03
$\sigma^{\mathrm{C1I1}}/\sigma^{\mathrm{SC}}$	0.32±0.04	0.29±0.05	0.17±0.02	0.12±0.02
$\sigma^{2E}/\sigma^{\mathrm{SC}}$	0.35±0.04	0.31±0.05	0.23±0.03	0.20±0.04
$\sigma^{\mathrm{TC}}/\sigma^{\mathrm{SC}}$	0.001±0.001	0.003±0.002	0.08±0.01	0.067±0.02
$\sigma^{\mathrm{C2I1}}/\sigma^{\mathrm{SC}}$	0.06±0.02	0.13±0.02	0.098±0.02	0.079±0.02
$\sigma^{\mathrm{C1I2}}/\sigma^{\mathrm{SC}}$	0.09±0.02	0.013±0.005	0.072±0.01	0.002±0.002
$\sigma^{3\mathrm{E}}/\sigma^{\mathrm{SC}}$	0.15±0.03	0.15±0.02	0.25±0.03	0.15±0.03
$\sigma^{\mathrm{QC}}/\sigma^{\mathrm{SC}}$	–	–	–	0.014±0.005
$\sigma^{\mathrm{C3I1}}/\sigma^{\mathrm{SC}}$	–	0.009±0.005	0.039±0.01	0.022±0.01
$\sigma^{\mathrm{C2I2}}/\sigma^{\mathrm{SC}}$		0.009±0.005	0.002±0.002	–
$\sigma^{\mathrm{C1I3}}/\sigma^{\mathrm{SC}}$	–	–	–	–
$\sigma^{4\mathrm{E}}/\sigma^{\mathrm{SC}}$	–	0.018±0.007	0.041±0.01	0.036±0.01

Table 5. Experimental cross-section ratios of $\sigma^{k\mathrm{E}}/\sigma^{\mathrm{SC}}$ ($k = 2$–4) for $q = 9$ isocharged sequence ions colliding with neon.

Projectile	Ne^{9+}	Si^{9+}	S^{9+}	Ar^{9+}	Ca^{9+}
configuration	$1s^1$	$1s^22s^22p^1$	$1s^22s^22p^3$	$1s^22s^22p^5$	$[Ne]1s^1$
energy/keV	4.5	4.5	4.5	4.5	4.5
velocity	0.42	0.42	0.42	0.42	0.42
$\sigma^{\mathrm{DC}}/\sigma^{\mathrm{SC}}$	0.029±0.01	0.019±0.01	0.027±0.01	0.058±0.02	0.023±0.005
$\sigma^{\mathrm{C1I1}}/\sigma^{\mathrm{SC}}$	0.28±0.02	0.26±0.02	0.34±0.03	0.45±0.03	0.27±0.03
$\sigma^{2\mathrm{E}}/\sigma^{\mathrm{SC}}$	0.31±0.02	0.28±0.02	0.37±0.03	0.51±0.04	0.29±0.03

Table 5. *Contiuned*

Projectile	Ne^{9+}	Si^{9+}	S^{9+}	Ar^{9+}	Ca^{9+}
configuration	$1s^1$	$1s^22s^22p^1$	$1s^22s^22p^3$	$1s^22s^22p^5$	$[Ne]1s^1$
energy/keV	4.5	4.5	4.5	4.5	4.5
velocity	0.42	0.42	0.42	0.42	0.42
σ^{TC}/σ^{SC}	0.001±0.001	0.004±0.003	0.008±0.005	0.031±0.01	0.007±0.005
$\sigma^{C2I1}/\sigma^{SC}$	0.084±0.02	0.22±0.02	0.11±0.02	0.12±0.02	0.039±0.01
$\sigma^{C1I2}/\sigma^{SC}$	0.12±0.02	0.051±0.02	0.061±0.02	0.093±0.02	0.009±0.005
σ^{3E}/σ^{SC}	0.21±0.03	0.28±0.03	0.18±0.03	0.24±0.03	0.055±0.01
σ^{QC}/σ^{SC}	–	–	–	0.011±0.005	–
$\sigma^{C3I1}/\sigma^{SC}$	0.001±0.001	0.002±0.002	0.02±0.01	0.064±0.02	0.019±0.005
$\sigma^{C2I2}/\sigma^{SC}$	0.012±0.005	0.025±0.01	0.10±0.02	0.11±0.02	0.012±0.005
$\sigma^{C1I3}/\sigma^{SC}$	0.013±0.005	0.001±0.001	0.008±0.005	–	–
σ^{4E}/σ^{SC}	0.026±0.01	0.028±0.01	0.13±0.02	0.19±0.03	0.031±0.007

Table 6. Experimental cross-section ratios of σ^{kE}/σ^{SC} ($k = 2$–4) for $q = 11$ isocharged sequence ions colliding with neon.

Projectile	Si^{11+}	Ar^{11+}	Ca^{11+}
configuration	$1s^22s^1$	$1s^22s^22p^3$	$1s^22s^22p^5$
energy/keV	5.5	5.5	5.5
velocity v_0	0.47	0.47	0.47
σ^{DC}/σ^{SC}	0.034±0.01	0.033±0.01	0.01±0.005
$\sigma^{C1I1}/\sigma^{SC}$	0.35±0.04	0.32±0.04	0.20±0.03
σ^{2E}/σ^{SC}	0.38±0.04	0.35±0.04	0.21±0.03
σ^{TC}/σ^{SC}	0.002±0.002	0.008±0.005	0.002±0.002
$\sigma^{C2I1}/\sigma^{SC}$	0.055±0.01	0.063±0.01	0.033±0.01
$\sigma^{C1I2}/\sigma^{SC}$	0.096±0.02	0.18±0.02	0.07±0.02
σ^{3E}/σ^{SC}	0.15±0.02	0.25±0.02	0.11±0.02
σ^{QC}/σ^{SC}	–	–	–
$\sigma^{C3I1}/\sigma^{SC}$	0.001±0.001	0.008±0.005	0.003±0.002
$\sigma^{C2I2}/\sigma^{SC}$	0.062±0.02	0.053±0.01	0.018±0.005
$\sigma^{C1I3}/\sigma^{SC}$	0.001±0.001	0.007±0.005	0.003±0.002
σ^{4E}/σ^{SC}	0.064±0.02	0.068±0.01	0.024±0.01

3.1. Multiple electron process

Figures 1(a)–1(c) show the cross section ratios of 2E, 3E and 4E to the SC process in the A^{q+}–Ne ($q = 6$–9, 11) collisions. As mentioned above, in order to identify the effect of ion velocity, the velocities are selected to be $0.49v_0$ and $0.35v_0$ for $q = 6$ sequence of ions, $0.43v_0$, $0.42v_0$ and $0.40v_0$ for $q = 7$ sequence of ions. The influence of velocity can be ignored in this case.[1,11] In the case of the 2E process, in Fig. 1(a), the value of σ^{2E}/σ^{SC} varies from 0.17 to 0.57, in a range of 0.4 as a function of the projectile number Z. In Fig. 1(b), the value of σ^{3E}/σ^{SC} varies from 0.014 to 0.25, while the value of σ^{4E}/σ^{SC} is in a range of 0.0–0.19 as displayed in Fig. 1(c). More peak-shape structures for Ar are located at $Z = 18$, which is caused by the core effect of ions. The projectile core factor fades away when the active electron number increases from 2 to 4.

The experimental and theoretical cross-section ratios σ^{kE}/σ^{SC} ($k = 2$–4) of multiple electron process to single capture for $q = 6$–9 and 11, are respectively displayed in Figs. 2(a)–2(e) as a function of projectile's atomic number Z. In the case of $q = 6$ isocharge sequence ions (C^{6+}, N^{6+}, O^{6+}, F^{6+}, Ne^{6+}, Ar^{6+} and Ca^{6+}), the value of cross-section ratio σ^{2E}/σ^{SC} is be-

tween 0.17 and 0.57 and their average value is ∼0.36, which is smaller than the predicted values which are 0.54, 0.50 and 0.55, as listed in Table 1. The values of cross-section ratio σ^{3E}/σ^{SC} are 0.14 for C^{6+}, N^{6+} and O^{6+}, and 0.06–0.10 for F^{6+}, Ne^{6+}, Ar^{6+} and Ca^{6+}. The average of these data is 0.10, which is less than half of the expected values, which are 0.33, 0.35 and 0.35 respectively. Figure 2(a) also shows that the cross-section ratio σ^{4E}/σ^{SC} of $q = 6$ isocharge sequence ions colliding with Ne changes from 0.01 to 0.06 with an average of 0.03. However the theoretical values of cross-section ratio σ^{4E}/σ^{SC} are 0.16, 0.10 and 0.15, at least three times as large as the experimental results. From Fig. 2(a), there is a tendency of increasing for the cross-section of 2E process as the projectile atomic number increases. On the other hand, tendencies of decreasing for the values of cross-section ratio σ^{3E}/σ^{SC} and σ^{4E}/σ^{SC} are shown in the same figure. Similar behaviours are observed in the collisions of C^{6+}, N^{6+} and O^{6+} with Ne. For Ar^{6+} and Ca^{6+}, 2E process is a domain reaction in the ME process however 4E process is not observed. All these phenomena are due to the influence of electron energy structure of projectile ions.

For $q = 7$ isocharge sequence ions (Fig. 2(b)), σ^{2E}/σ^{SC} values of 0.50, 0.45, 0.53, 0.38, 0.45 and 0.22 are plotted for O^{7+}, F^{7+}, N^{7+}, S^{7+}, Ar^{7+} and Ca^{7+}. The average value of the experimental data is 0.42, while the calculations are 0.55, 0.50 and 0.55. 2E process has a downward tendency as the projectile atomic number increases. The value of σ^{3E}/σ^{SC} varies from 0.01 to 0.25, reaching a maximum of 0.25 at $Z = 16$ with an average value of 0.08. The theoretical values of σ^{3E}/σ^{SC} are 0.19, 0.14 and 0.20. In C^{6+}, N^{6+} and O^{6+} colliding with neon, the 2E cross sections are three times as large as the 3E, but in O^{7+}, F^{7+} and Ne^{7+} colliding with neon, the 2E cross sections are 7–50 times larger than 3E cross sections. As we know, the second ionisation energy of neon is very close to the $n = 4$ level-group of $q = 7$ ions (O^{7+}, F^{7+} and Ne^{7+}). Hence it is resonant transfer, which enhances 2E process strongly in the collision of O^{7+}, F^{7+} and Ne^{7+}. Similar phenomena can also be found in argon target collisions. The relative cross-section value of 4E process changes from 0.002 to 0.082 with an average value of 0.022. It is smaller than the predicted values which are 0.070, 0.097 and 0.146 respectively. Similar indications of σ^{kE}/σ^{SC} (k = 2–4) have been observed for O^{7+}, F^{7+} and Ne^{7+}, but not for S^{7+}, Ar^{7+} and Ca^{7+}, which can be explained as being due to the fact that the vacant level structures are similar for O^{7+}, F^{7+} and Ne^{7+} and are distinct for S^{7+}, Ar^{7+} and Ca^{7+}. From the discussion above, it is known that theoretical prediction overestimates the multi-electron process.

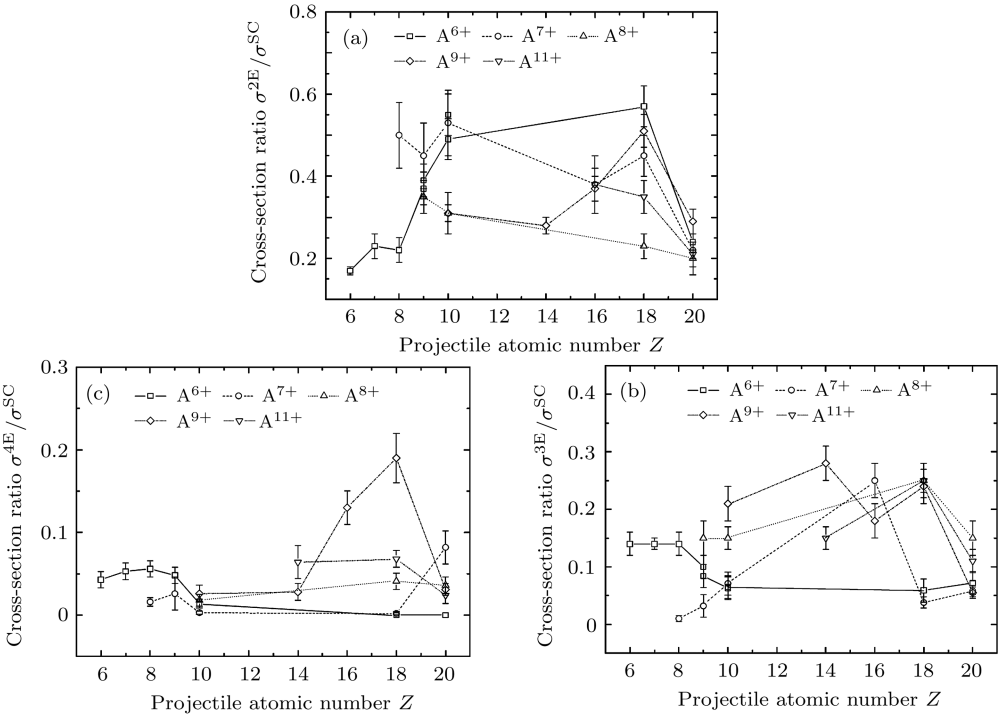


Fig. 1. Measured values of cross-section ratio σ^{kE}/σ^{SC} (k = 2–4) as a function of projectile atomic number Z for the collision of isocharge sequence ions with Ne.

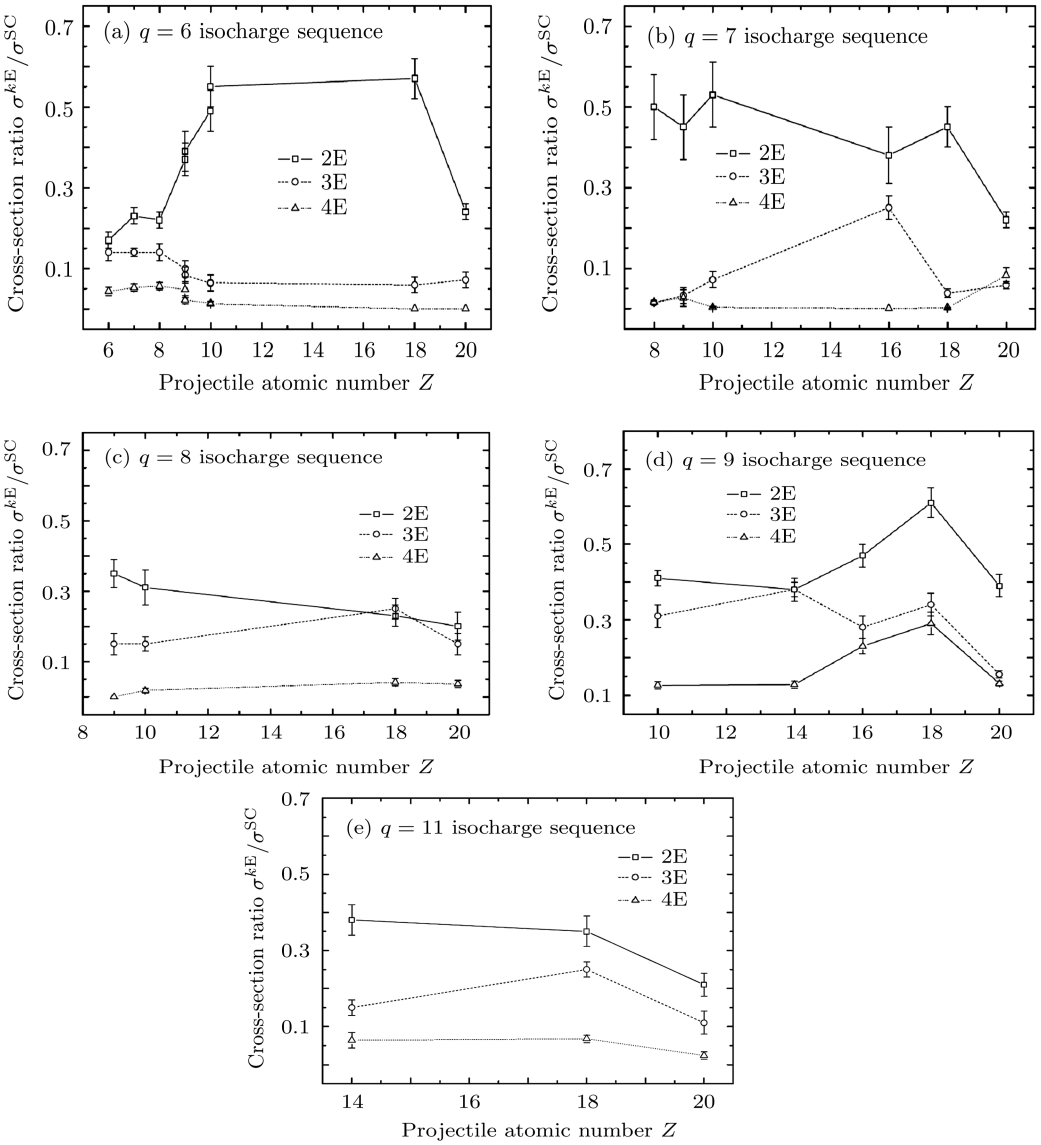


Fig. 2. Experimental and theoretical values of cross-section ratio (MCBM, ECBM and SSL) σ^{kE}/σ^{SC} ($k = 2$–4) of ME process to single capture for $q = 6$(a), 7(b), 8(c), 9(d) and 11(e), as a function of projectile atomic number Z, where k is the number of active electrons.

Experimental data and calculations of σ^{kE}/σ^{SC} ($k = 2$–4) for the case of $q = 8$ isocharge sequence ions are displayed in Fig. 2(c). As shown in Fig. 2(c), σ^{2E}/σ^{SC} decreases from 0.35 to 0.20 as the projectile atomic number increases. The model prediction is around 0.50–0.55, about twice larger than the average value of experimental data of ∼0.27. The experimental measurement determines the values of σ^{3E}/σ^{SC} to be 0.15 for F^{8+}, Ne^{8+}, and Ca^{8+}, and 0.25 for Ar^{8+}. The average of experimental results is 0.18, which is smaller than the theoretical values of 0.32, 0.36 and 0.35 given by three models. The 4E process is very weak due to the competition between all charge transfer channels, just ∼ 2.2% of σ^{SC}, and there is no 4E process for F^{8+} in our case. Theoretical models still give higher predictions to the 4E process. For the projectile charge state $q = 8$, the 2E process becomes weaker, while the 3E process turn stronger. The weight of them in multi-electron process can be compared with each other.

In Fig. 2(d), the measured values of σ^{2E}/σ^{SC} are 0.31, 0.28 and 0.37 for Ne^{9+}, Si^{9+}, S^{9+} respectively, they go up to a maximum of 0.51 for Ar^{9+}, finally declines down to 0.29 for Ca^{9+}. However the theoretical values are 0.56, 0.50 and 0.55. Figure 2(d) also shows the fluctuation of σ^{3E}/σ^{SC} to be between 0.055 and 0.28 with the constant values of 0.32, 0.36 and 0.35 predicted by the models. The value of σ^{4E}/σ^{SC} varies from 0.026 to 0.19 with an average of 0.081 and the theoretical models predict the ratio values to be 0.18,

0.13 and 0.20. Comparing σ^{4E}/σ^{SC} with σ^{2E}/σ^{SC}, it is known that the cross sections of 4E process follow the trend of cross sections of 2E process. For Si^{9+}, the cross section of 3E process is almost equal to the one of 2E process. The total cross section of ME is quite large for Ar^{9+}, about 97% of SC. A peak-shape structure is shown in the figure when the projectile is Ar^{9+}.

The projectiles of charge state $q = 11$, only are selected to be three kinds of ions, i.e., Si^{11+}, Ar^{11+} and Ca^{11+} due to the limit of ECRIS. The values of σ^{2E}/σ^{SC} are 0.38, 0.35 and 0.21 for Si^{11+}, Ar^{11+} and Ca^{11+}, with the predictions being 0.55, 0.50 and 0.55. The value of σ^{3E}/σ^{SC} is between 0.11 and 0.25. Three models predict the values of σ^{3E}/σ^{SC} to be 0.33, 0.36 and 0.35 respectively for Si^{11+}, Ar^{11+} and Ca^{11+} which are about twice as large as the experimental mean value of 0.19. The experimental measurements of σ^{4E}/σ^{SC} which are 0.064, 0.068 and 0.024 for Si^{11+}, Ar^{11+} and Ca^{11+} respectively, each show a flat curve as the projectile atomic number increases. The constants of 0.17, 0.13 and 0.20 are given by the calculations for the projectile charge state q of 11. From Fig. 2(e), the cross sections of 2E process for Si^{11+} and Ar^{11+} are remarkably larger than for Ca^{11+}. For 3E process, the Ar^{11+} cross section is higher than for the others.

The ME processes have been extensively studied over past several decades. However, few cross section measurements in collision of HCIs with Ne target have been made.[18,41,42] The collision systems were Ar^{q+}–Ne in Refs. [41] and [42] and I^{q+}–Ne in Ref. [18] at keV energy. Additionally, for the collision system of Ar^{q+}–Ne, the cross sections of a full set of reaction processes are available just for two-election transfer, not for more than two-electron transfer. For these reasons, we compare our data of Ar^{q+}–Ne with reported data for two-electron transfer process. Figure 3 shows the comparison between our results and the data from Refs. [18], [41] and [42]. The cross section ratio of σ^{2E}/σ^{SC} for our experiment is in good agreement with the results given in Refs. [41] and [42]. As the projectile charge q increases, the σ^{2E}/σ^{SC} ratio increases rapidly, and reaches a maximum value at $q = 5$, then decreases slowly. It implies that 2E process will be strongest when q is ∼5–6.

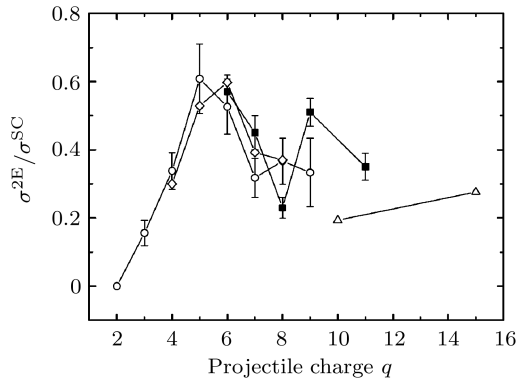


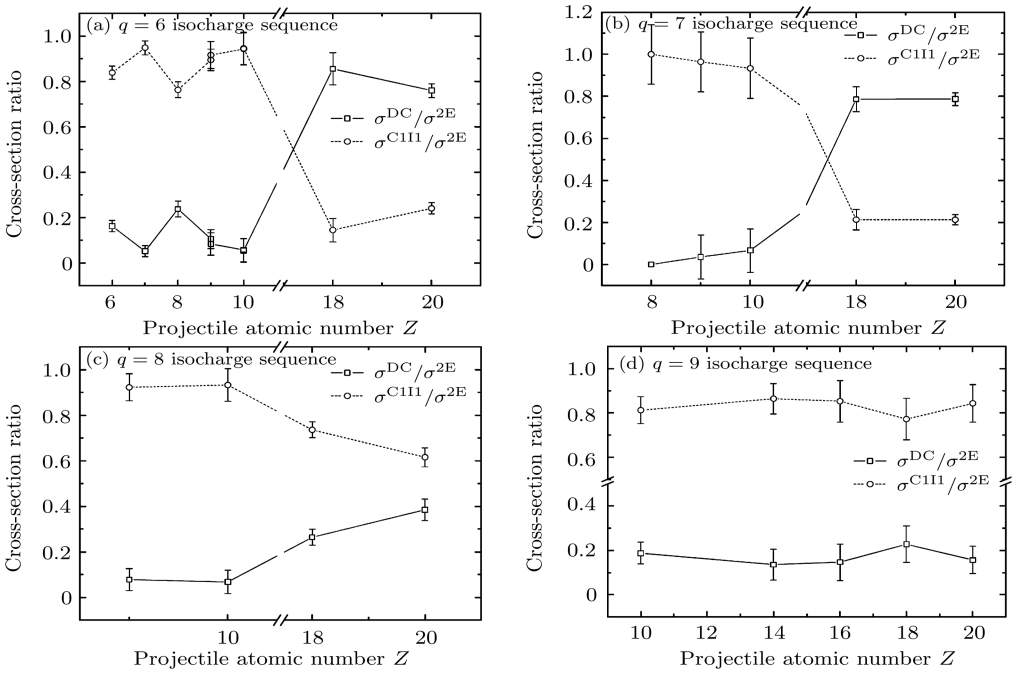
Fig. 3. Comparison among present results ($4q$ keV, ■), the results of Liljeby *et al.*[41] ($1.8q$ keV, ○), the results of Justiniano *et al.*[42] (1 keV, ◇), and the results of Nakamura *et al.*[18] ($1.5q$ keV, Δ) for Ar^{q+}–Ne cross section ratio σ^{2E}/σ^{SC}.

3.2. Partial reaction channels among mutliple electron processes

The decay of multi-excited projectiles after collision is important information about the collision of HCIs with rare gas target. The branching ratios involve the information about the decay of multiply-excited ions. The values of σ^{DC}/σ^{2E}, $\sigma^{C1I1}/\sigma^{2E}$ in the measurement of isocharge sequence ions (q = 6–9,11) colliding with Ne, as a function of the projectile atomic number, are plotted in Fig. 4(a)–4(e). In our case, the true double-electron ionisation is not determined so that the 2E process includes DC and the C1I1 process, that means $\sigma^{2E} = \sigma^{DC} + \sigma^{C1I1}$. With the projectile charge state $q = 6$ and 7, for DC and C1I1 processes, the values of σ^{DC}/σ^{2E} and σ^{DC}/σ^{2E} keep small variations as the projectile atomic numbers are between 6 and 10, and between 18 and 20 respectively. $\sigma^{C1I1}/\sigma^{2E}$ which is about 0.90, is quite larger than σ^{DC}/σ^{2E} which is about 0.10, when the projectile atomic number is between 6 and 10. However, $\sigma^{C1I1}/\sigma^{2E}$ which is about 0.20, is remarkably smaller than σ^{DC}/σ^{2E} which is about 0.80, when the projectile atomic number is between 18 and 20. A reverse tendency can be seen as the projectile atomic number changes from 10 to 18. Similar behaviours are shown in Fig. 4(c) where the ion charge state is 8. When the projectile atomic number is larger than 10, the value of $\sigma^{C1I1}/\sigma^{2E}$ decreases from about 0.9 to about 0.6, while the value of σ^{DC}/σ^{2E} increases from about 0.10 to about 0.40. Comparing Fig. 4(c) with Figs. 4(a) and 4(b), it can be found the curve of σ^{DC}/σ^{2E} in Fig. 4(c) does not cross with the one of $\sigma^{C1I1}/\sigma^{2E}$, which is different form the scenarios in Figs. 4(a) and 4(c). What is more, as illustrated in Figs. 4(d) and

4(e), the values of $\sigma^{\rm DC}/\sigma^{\rm 2E}$ and $\sigma^{\rm C1I1}/\sigma^{\rm 2E}$, independent of ion charge state q, are about 0.90 and 0.10 respectively. One conclusion can be made that the reverse tendency is caused by the ion core effect which fades away as ion charge state q increases. When the projectile atomic number is between 6 and 10, C1I1 is absolutely the domain process among 2E process. And for the Ar and Ca projectile ions, which channel is the domain channel depends on the projectile charge state q, which is shown in Figs. 4(a)–4(e). It is found that the decay of doubly-excited ions is dependent on electronic vacancy of projectile. For the projectiles with fill K-shell, C1I1 is dominant in 2E process. However, for the projectiles with fill M-shell, branching ratio of C2 has large value, compared with that for C1I1. A similar phenomenon can be seen, and the same conclusion can be made in the branching ratios of 3E process from Fig. 5.

Figures 5(a)–5(e) show the measured values of $\sigma^{\rm TC}/\sigma^{\rm 3E}$, $\sigma^{\rm C2I1}/\sigma^{\rm 3E}$ and $\sigma^{\rm C1I2}/\sigma^{\rm 3E}$ for the sequence of isocharge ions (q = 6–9, 11) colliding with Ne. 3E process has four possible reaction channels, *i.e.*, TC, C2I1, C1I2 and I3. However, the three-electron ionisation process is not observed in our experimental measurement so that the total cross section of 3E is the sum of the cross sections of TC, C2I1, C1I2, i.e. $\sigma^{\rm 3E} = \sigma^{\rm TC} + \sigma^{\rm C2I1} + \sigma^{\rm C1I2}$. For the A^{6+} ions, the cross-section ratios of $\sigma^{\rm TC}/\sigma^{\rm 3E}$ and $\sigma^{\rm C2I1}/\sigma^{\rm 3E}$ fluctuate between 0.014 and 0.27, between 0.54 and 0.73 respectively, as the projectile atomic number increases from 6 to 10. But for Ar^{6+} and Ca^{6+}, the ratios of $\sigma^{\rm TC}/\sigma^{\rm 3E}$, are 0.58 and 0.65 respectively and ratios of $\sigma^{\rm C2I1}/\sigma^{\rm 3E}$ are both 0.18. A reverse trend between $\sigma^{\rm TC}/\sigma^{\rm 3E}$ and $\sigma^{\rm C2I1}/\sigma^{\rm 3E}$ is also observed as the projectile atomic number changes from 10 to 18. The result is caused by the influence of projectile core properties. For $\sigma^{\rm C2I1}/\sigma^{\rm 3E}$, a downward tendency is shown in Fig. 5(a). From Figs. 5(a)–5(e), we can see that TC becomes stronger and stronger for q = 6, 8 and 9, and fluctuates around a constant for q = 7 and 11, as the projectile atomic number increases. The larger the projectile charge state q is, the lower will the value of $\sigma^{\rm TC}/\sigma^{\rm 3E}$ be. The cross-section ratio $\sigma^{\rm C2I1}/\sigma^{\rm 3E}$ fluctuates around a constant with the increase of projectile atomic number for q = 7–9 and 11. For q = 6–9, $\sigma^{\rm C2I1}/\sigma^{\rm 3E}$ shows a downward trend when the projectile ion becomes heavy. The C1I2 process becomes weak with the increase of projectile atomic number in the case of q = 6–9, while it is independent of the variety of projectile ions when the projectile charge state is 11. With the increase of projectile charge state q, TC and C2I1 processes become weak, while C1I2 becomes strong. The cross sections of C2I1 are greater than the ones of TC and C1I2 over the range of projectile charge state q from 6 to 9. However, when the projectile charge state q is goes up to 11, C1I2 is the strongest partial channel in 3E process. In the case of 3E process, there is an effect of projectile core which can be observed when the projectile charge state q is equal to 6.



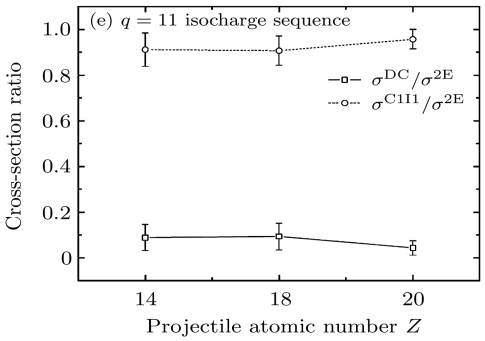


Fig. 4. Measured data of σ^{DC}/σ^{2E} and $\sigma^{C1I1}/\sigma^{2E}$ as a function of projectile atomic number Z in the case of projectile charge state $q = 6$–9, 11.

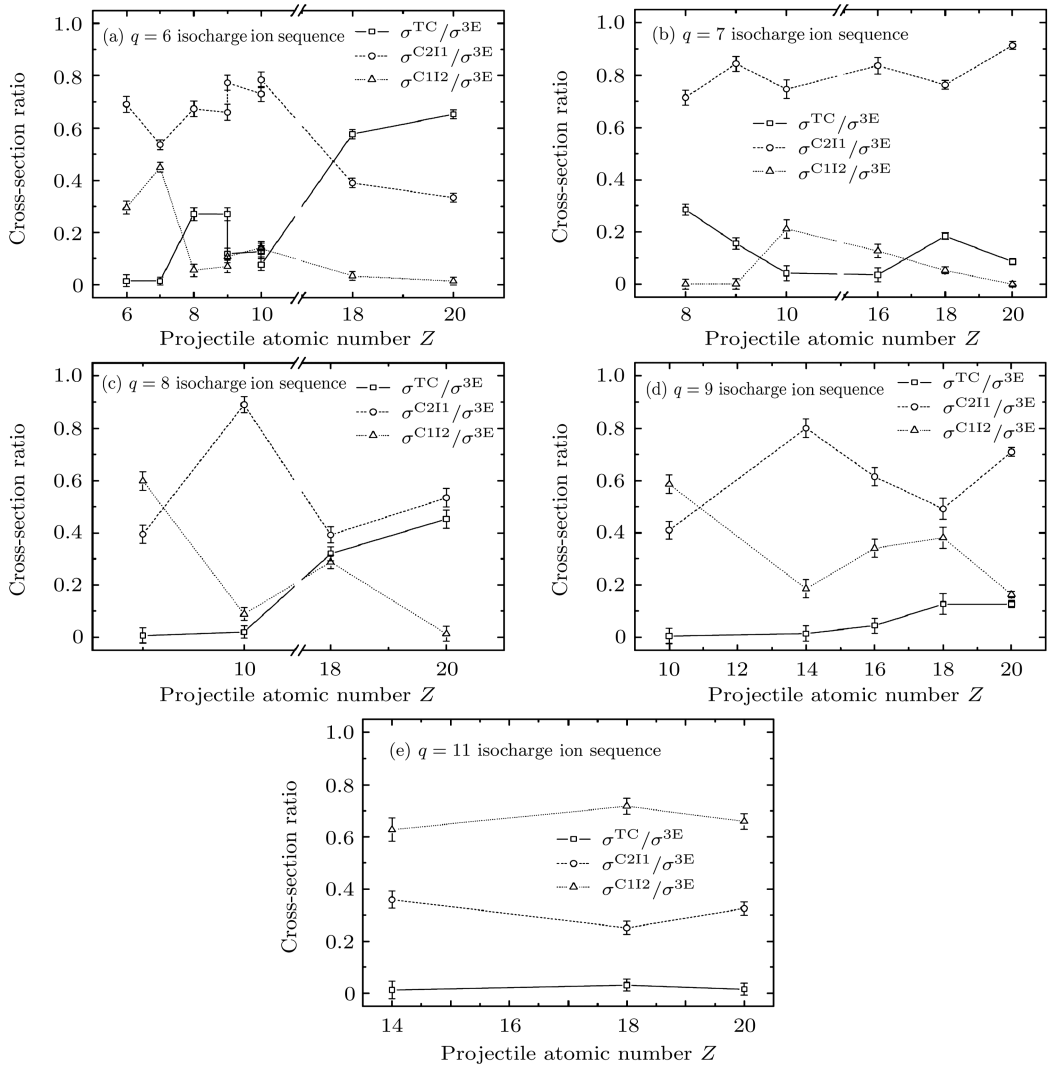


Fig. 5. Measured values of σ^{TC}/σ^{3E}, $\sigma^{C2I1}/\sigma^{3E}$ and $\sigma^{C1I2}/\sigma^{3E}$ for the sequence of isocharge ions ($q = 6$–9, 11) colliding with Ne.

In 2E process, two electrons are transferred from Ne target to high energy levels of projectile, and then deexcited through either radiative decay or single Auger decay. The comparison of branching ratio of 2E between present work and Refs. [18], [41] and [42] is shown in Figs. 6(a) and 6(b). As seen in Fig. 6, when the projectile charge state q increases, the branching ratio of DC drops down to 0.1 quickly, while the one of C1I1 goes up to 0.9. These results coincide very well with the calculations and experimental data in Ref. [43]. It suggests that both occupied levels and projectile core states must be considered.[16,17]

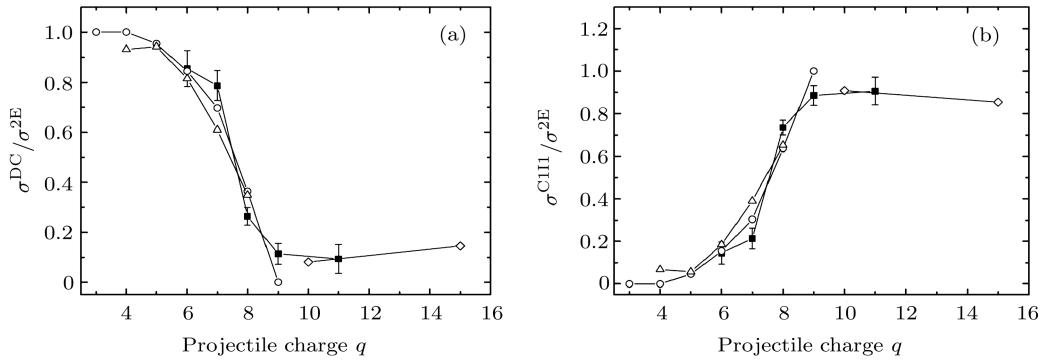


Fig. 6. Comparison among the present results ($4q$ keV, ■), the results of Liljeby *et al.*[41] ($1.8q$ keV, ◯), the results of Justiniano *et al.* [42] (1 keV, ◇), and the results of Nakamura *et al.*[18] ($1.5q$ keV, Δ) for Ar^{q+}–Ne cross section ratios of σ^{DC}/σ^{2E} and $\sigma^{C1I1}/\sigma^{2E}$.

4. Conclusions

In this work, the ME processes in the collisions of $q = 6$–9 and 11 isocharged sequence ions with Ne are investigated in the keV/u region. The cross-section ratios of 2E, 3E and 4E to the single electron capture process, and the partial ratios of different reaction channels to the relevant multi-electron process have been measured using position sensitive and TOF techniques. The cross-section ratios of 2E, 3E and 4E to SC indicate the electron redistribution between the projectile and target during the ion–atom interaction. The partial ratios of different reaction channels to the relevant multi-electron process exhibit the electron-electron interaction during the projectile relaxation.

The present work shows that 2E process is a domain reaction channel among the multi-electron processes, 3E channel is weaker than 2E, and 4E channel is very small. This result is in good agreement with the predictions by MCBM, ECBM and SSL. However, by comparison with the experimental data, theoretical models overestimate the multi-electron process. The more the active electron number is, the more the theoretical models overestimate. The reason is that MCBM, ECBM and SSL characterise the projectile ion with only its charge state q so that different ions in an isocharged sequence cannot be distinguished from each other. In the ME process, transfer ionisation is dominant and the pure electron capture is negligible while the direct ionisation is not observed. It indicates that the active electrons are first captured to multi-excited state of projectile and then go to the ground state through radiation or to the continuum state through emission after the interactions between the electrons. The experimental data suggest that the cross-section ratios of ME process to single capture and the partial ratios among the relevant multi-electron process are strongly affected by the projectile core properties. Multi-excited ion decay is strongly dependent on electron vacancy of projectile. That means that the vacant energy level structure of the projectile ions has a strong influence on the electron redistribution and the projectile relaxation. The result shows that the projectile core effect fades away as the charge state of projectile ions increases, which indicates a character that the projectile core effect becomes weak for those sufficiently charged ions, where the electrons are captured to the high-level states and the spontaneous ionisation becomes dominant in the relaxation of projectile. The results of present work are compared with previous experimental data and they are in good agreement with each other.

References

[1] Yu D Y, Cai X H, Lu R C, Ruan F F, Shao C J, Zhang H Q, Cui Y, Lu J, Xu X, Shao J X, Ding B W, Yang Z H, Chen X M and Liu Z Y 2007 *Phys. Rev.* A **76** 022710
[2] Drawin H W 1981 *Phys. Scr.* **24** 622
[3] Niehaus A 1986 *J. Phys.* B **19** 2925
[4] Herrmann R, Prior M H, Dörner R, Schmidt-Böcking H, Lyneis C M and Wille U 1992 *Phys. Rev.* A **46** 5631
[5] Nagy L 1999 *Nucl. Instr. Meth.* B **154** 123
[6] Ruan F F, Cai X H, Yu D Y, Lu R C, Shao C J, Lu J, Cui Y, Shao J X, Xu X, Zhang H Q, Ding B W, Yang Z H and Chen X M 2006 *Chin. Phys. Lett.* **23** 95
[7] Ruan F F, Cai X H, Yu D Y, Lu R C, Shao C J, Lu J, Cui Y, Shao J X, Xu X, Zhang H Q, Ding B W, Yang Z H and Chen X M 2007 *Chin. Phys. Lett.* **24** 921
[8] Salmoun A, Brédy R, Bernard J, Chen L and Martin S 2008 *Euro. Phys. J.* D **47** 55

[9] Arianer J and Geller R 1981 *Annu. Rev. of Nucl. Part. Sci.* **31** 19
[10] Janev R K and Presnyakov L P 1981 *Phys. Rep.* **70** 1
[11] Barat M and Roncin P 1992 *J. Phys.* B **25** 2205
[12] Cocke C L, DuBois R, Gray T J, Justiniano E and Can C 1981 *Phys. Rev. Lett.* **46** 1671
[13] Müler A, Groh W and Salzborn E 1983 *Phys. Rev. Lett.* **51** 107
[14] Bárány A, Astner G, Cederquist H, Danared H, Huldt S, Hvelplund P, Johnson A, Knudsen H, Liljeby L and Rensfelt K G 1985 *Nucl. Instr. Meth.* B **9** 397
[15] Martin S, Denis A, Ouerdane Y, Salmoun A, EI Motassadeq A, Désesquelles J, Druetta M, Church D and Lamy T 1990 *Phys. Rev. Lett.* **64** 2633
[16] Vaeck N and Hansen J E 1991 *J. Phys.* B **24** L469
[17] van der Hart H W and Hansen J E 1993 *J. Phys.* B **26** 641
[18] Nakamura N, Currell F J, Danjo A, Kimura M, Matsumoto A, Ohtani S, Sakaue H A, Sakurai M, Tawara H, Watanabe H, Yamada I and Yoshino M 1995 *J. Phys.* B **28** 2959
[19] Sakaue H A, Tawara H, Yamada I, Hosaka K, Krok F, Currell F J, Nakamura N, Ohtani S, Watanabe H, Danjo A, Kimura M, Matsumoto A, Sakurai M and Yoshino M 1997 *Phys. Scr.* **T73** 182
[20] Knoop S, Turkstra J W, Morgenstern R, Olson R E and Hoekstra R 2003 *Nucl. Instr. Meth.* B **205** 560
[21] Tawara H, Takács E, Suta T, Makónyi K, Ratliff L P and Gillaspy J D 2006 *Phys. Rev.* A **73** 012704
[22] Hoshino M, Kambara T, Kanai Y, Schuch R and Yamazaki Y 2007 *Phys. Rev.* A **75** 032722
[23] Tan J, Lin C D and Kimura M 1987 *J. Phys.* B **20** L91
[24] Mann R and Schulte H 1987 *Z. Phys.* D **4** 343
[25] Kimura M, Nakamura N, Watanabe H, Yamada I, Danjog A, Hosaka K, Matsumoto A, Ohtani S, Sakaue H A, Sakuai M, Tawara H and Yoshino M 1995 *J. Phys.* B **28** L643
[26] Chaudhuri C, Sanyal S and Rai Dastidar T K 1995 *Phys. Rev.* A **52** 1137
[27] Selberg N, Biedermann C and Cederquist H 1997 *Phys. Rev.* A **56** 4623
[28] Lugosi L and Sarkadi L 2003 *Nucl. Instr. Meth.* B **205** 591
[29] Santos A C F and DuBois R D 2004 *Phys. Rev.* A **69** 042709
[30] Chen L, Chen X and Liu Z 2008 *Phys. Lett.* A **372** 681
[31] Bohr N and Lindhard J 1954 *K. Dan. Vidensk. Selsk. Mat. Fys. Medd.* **28** 7
[32] Tolstikhina I Y, Tolstikhin O I and Tawara H 1998 *Phys. Rev.* A **57** 4387
[33] Ito H, Chihara Y, Suzuki Y, Hirayama T and Koizumi T 2007 *J. Phys. Conf. Ser.* **58** 311
[34] Becker R L, Ford A L and Reading J F 1980 *J. Phys.* B **13** 4059
[35] Beijers J P M, Hoekstra R, Schlatmann A R, Morgenstern R and de Heer F J 1992 *J. Phys.* B **25** 463
[36] de Nijs G, Folkerts H O, Hoekstra R and Morgenstern R 1996 *J. Phys.* B **29** 85
[37] Fléchard X, Harel C, Jouin H, Pons B, Adoui L, Frémont F, Cassimi A and Hennecart D 2001 *J. Phys.* B **34** 2759
[38] Bernard J, Brédy R, Martin S, Chen L, Désesquelles J and Buchet-Poulizac M C 2002 *Phys. Rev.* A **66** 013209
[39] Cai X H, Yu D Y, Lu R C, Cao Z R, Yang W, Shao C J, Chen X M and Ma X W 2004 *Nucl. Instr. Meth.* B **225** 185
[40] Cai X H, Yu D Y, Cao Z R, Lu R C, Yang W, Shao C J and Chen X M 2004 *Chin. Phys.* **13** 1679
[41] Liljeby L, Astner G, Bárány A, Cederquist, Danared H, Huldt S, Hvelplund P, Johnson A, Knudsen H and Rensfelt K G 1986 *J. Phys.* B **33** 310
[42] Justiniano E, Cocke C L, Gray T J, DuBois R D and Can C 1981 *Phys. Rev.* A **24** 2953
[43] Sakaue H A, Danjo A, Hosaka K, Kato D, Kimura M, Matsumoto A, Nakamura N, Ohtani S, Sakurai M, Tawara H, Yamada I and Yoshino M 2004 *J. Phys.* B **37** 403